GEOPHYSICS, VOL. 59, NO. 12 (DECEMBER 1994); P. 1894–1901, 5 FIGS.

Implementation of the Kirchhoff integral for elastic waves in staggered-grid modeling schemes

Rune Mittet*

ABSTRACT

Implementation of boundary conditions in finite-difference schemes is not straightforward for the elastic wave equation if a staggered grid formulation is used. Reverse time migration of VSP data requires a proper description of the recording surface so as not to excite false P- and S-waves. Such contributions may cause artifacts in the imaging procedure. The boundary conditions for the elastic stress tensor can be implemented numerically in a staggered coarse grid modeling scheme by using band-limited spatial delta-functions and band-limited first-order derivatives of these spatial delta-functions. A representation theorem for elastic waves is derived to test the implementation of the spatial part of the boundary condition. The implementation is tested in a 2-D numerical experiment for a closed, but curved, boundary S enclosing a volume V. The test condition is that within the volume V, the difference between the forward modeled field and the retropropagated field should be equal to zero. Both P- and S-waves are properly recovered in a 2-D reverse time modeling example. The numerical artifacts related to the proposed spatial approximation of the boundary condition are found to be negligible.

INTRODUCTION

The combination of staggered grid methods (Madariaga, 1976, Virieux, 1984; 1986) with coarse grid methods (Gazdag, 1981; Kosloff and Baysal, 1982; Holberg, 1987; Levander, 1988; Fornberg, 1990) has improved the accuracy of seismic wave modeling. However, the difficulties of specifying the desired geometrical positions increase as the spatial sampling intervals come closer to a typical wavelength, and when field components are defined on shifted grids. Thus, for coarse grid methods, internal medium interfaces that are not aligned with the grid cause more problems than interfaces aligned with the grid. These problems occur because the staircase appearance of nonaligned interfaces generates unwanted diffractions. Similar effects may appear when boundary conditions are implemented in an elastic staggered grid scheme. Mispositioning contributions with half a grid step may degrade the modeling results significantly. Consistent implementation of boundary conditions is even more important in an elastic scheme than in an acoustic scheme since incorrectly implemented P-waves will introduce false S-waves in addition to false P-waves and vice versa. Retropropagation of the recorded wavefield is important in reverse time migration of vertical seismic profiling (VSP) data (Chang and McMechan, 1986; Mittet and Helgesen, 1992). False P- and S-waves generated when retropropagating the recorded data may correlate with the forward propagated field and degrade the final image.

A rigorous test of the implementation of the boundary condition for elastic waves can be done assuming a closed surface with a complete set of boundary conditions followed by a comparison of the forward propagated field with the retropropagated field. A poor approximation of the spatial part of the boundary condition will give rise to a difference between the forward propagated and retropropagated wavefield. In the following, a representation theorem for the elastic stress field is derived. The surface integral term of this representation theorem is an important part of any migration scheme (Kirchhoff integral in the acoustic case). A way of implementing this surface integral term for elastic waves in a staggered coarse grid modeling scheme is proposed. Results from a numerical experiment are shown, where the proposed implementation of the spatial boundary conditions is tested in 2-D with a closed surface having both plane and curved segments. The curved recording surface segment is chosen to verify that the proposed method works also for VSP data recorded in a deviated well. To be able to identify the different wavefield contributions, a homogeneous medium with a free surface outside the volume where the wavefield is reconstructed is used. The representation

Manuscript received by the Editor December 18, 1992; revised manuscript received June 16, 1994.
*IKU Petroleum Research, N-7034 Trondheim, Norway.

theorem developed here, however, is for a generally inhomogeneous medium. It can be inferred from this representation theorem that if the density is known on the recording surface and the medium where the wave is to be reconstructed is known, then the internal complexity of this medium is irrelevant as long as the wave simulation scheme provides the proper solution in this medium.

REPRESENTATION THEOREM FOR THE STRESS FIELD

In the following, the Einstein summation convention is used. Starting from the equation of motion

$$\rho(\mathbf{x})\partial_t^2 u_i(\mathbf{x}, t) = \partial_j \sigma_{ij}(\mathbf{x}, t) + f_i(\mathbf{x}, t), \quad (1)$$

and the constitutive relation

$$\sigma_{ij}(\mathbf{x}, t) = c_{ijk\ell}(\mathbf{x})\varepsilon_{k\ell}(\mathbf{x}, t), \quad (2)$$

the wave equation for the stress field is obtained as

$$s_{pqij}(\mathbf{x})\partial_t^2 \sigma_{ij}(\mathbf{x}, t) - \tfrac{1}{2}[\partial_p[\rho^{-1}(\mathbf{x})\partial_k \sigma_{qk}(\mathbf{x}, t)] + \partial_q[\rho^{-1}(\mathbf{x})\partial_k \sigma_{pk}(\mathbf{x}, t)]] = M_{pq}(\mathbf{x}, t), \quad (3)$$

where

$$M_{pq}(\mathbf{x}, t) = \tfrac{1}{2}[\partial_p[\rho^{-1}(\mathbf{x}) f_q(\mathbf{x}, t)] + \partial_q[\rho^{-1}(\mathbf{x}) f_p(\mathbf{x}, t)]]. \quad (4)$$

Here $\rho(\mathbf{x}, t)$ is the density, $c_{pqij}(\mathbf{x})$ is the Hooke's tensor, $u_i(\mathbf{x}, t)$ is a component of the displacement vector, $\sigma_{ij}(\mathbf{x}, t)$ is a component of the stress tensor, and $f_i(\mathbf{x}, t)$ is a component of the body-force distribution vector. The strain tensor is

$$\varepsilon_{k\ell} = \tfrac{1}{2}[\partial_k u_\ell(\mathbf{x}, t) + \partial_\ell u_k(\mathbf{x}, t)]. \quad (5)$$

Here ∂_t is the partial derivative with respect to time, and ∂_i is the partial derivative with respect to spatial coordinates. The elastic parameters are related by

$$s_{ijpq}(\mathbf{x}) c_{pqk\ell}(\mathbf{x}) = \tfrac{1}{2}[\delta_{ik}\delta_{j\ell} + \delta_{i\ell}\delta_{jk}]. \quad (6)$$

Equation (3) may be obtained by differentiating equation (2) twice with respect to time and then multiplying both sides with the tensor $s_{ijpq}(\mathbf{x})$. Using equation (5), the particle acceleration obtained from equation (1) is inserted. Based on equation (3), the Green's tensor for the stress field, $G_{ijnm}(\mathbf{x}, t|\mathbf{x}', t')$, is given by

$$s_{pqij}(\mathbf{x})\partial_t^2 G_{ijnm}(\mathbf{x}, t|\mathbf{x}', t') - \tfrac{1}{2}[\partial_p[\rho^{-1}(\mathbf{x})\partial_k G_{qknm}(\mathbf{x}, t|\mathbf{x}', t')] + \partial_q[\rho^{-1}(\mathbf{x})\partial_k G_{pknm}(\mathbf{x}, t|\mathbf{x}', t')]] = \tfrac{1}{2}[\delta_{pm}\delta_{qn} + \delta_{qm}\delta_{pn}]\delta(\mathbf{x} - \mathbf{x}')\delta(t - t'). \quad (7)$$

To obtain the representation theorem for the stress field in the desired form, homogeneous boundary conditions are assumed. This may not always be a property of the recording surface used to reconstruct the field from the boundary conditions. One way to circumvent this problem is to introduce the recording surface as an internal artificial surface that is transparent to the Green's tensor and its derivatives (Aki and Richards, 1980) and assume homogeneous boundary conditions or the Sommerfeld radiation condition on some outer surface, which for practical purposes will be the edges of the numerical model. Hence, homogeneous boundary conditions are assumed on a closed surface S_0 surrounding the internal recording surface S (see Figure 1) transparent to the Green's tensors and their partial derivatives. Then spatial reciprocity relations for the Green's tensors in the total volume enclosed by S_0 may be used. This volume also includes the volume enclosed by the recording surface S, thus, inhomogenous boundary conditions on S may be used, without sacrificing the spatial reciprocity relations for the Green's tensor. This assumption is verified by the numerical example given in this paper.

The representation theorem for the stress field can be obtained from equations (3) and (7). A detailed derivation of the acoustic representation theorem is given in Morse and Feshbach (1953). The elastic representation theorem can be derived in a similar manner and the stress tensor is

$$\sigma_{mn}(\mathbf{x}, t) = \int_0^{t^+} dt' \int d^3x' G_{mnij}(\mathbf{x}, t - t'|\mathbf{x}', 0) M_{ij}(\mathbf{x}', t') + \int_0^{t^+} dt' \oint_S dS(\mathbf{x}_r) \left\{ G_{mnij}(\mathbf{x}, t - t'|\mathbf{x}_r, 0) n_i a_j(\mathbf{x}_r, t') - [\partial_i^r G_{mnij}(\mathbf{x}, t - t'|\mathbf{x}_r, 0)] \frac{n_p \sigma_{jp}(\mathbf{x}_r, t')}{\rho(\mathbf{x}_r)} \right\} + \int d^3x' \{[\partial_{t'} G_{mnij}(\mathbf{x}, t - t'|\mathbf{x}', 0)] \varepsilon_{ij}(\mathbf{x}', t')$$

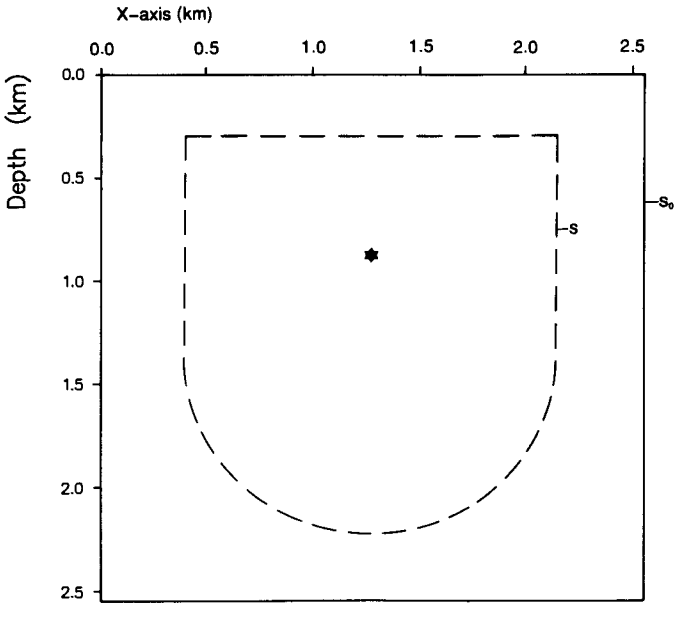

FIG. 1. The model used in the numerical experiment. P-wave velocity is 2000 m/s, S-wave velocity is 1200 m/s, and density is 2.0 g/cm^3. The top surface is a free surface, the rest of the model is surrounded by absorbing boundaries. The source position is marked with a star. The fields $a_x^n(i_r, j_r)$, $a_z^n(i_r, j_r)$, $t_x^n(i_r, j_r)$, and $t_z^n(i_r, j_r)$ are recorded on the surface S. The numerical grid is contained within the surface S_0.

$$- G_{mnij}(\mathbf{x}, t - t'|\mathbf{x}', 0)\partial_{t'}\varepsilon_{ij}(\mathbf{x}', t')\}|_0^{t^+}, \quad (8)$$

where t^+ means $t + \varepsilon$, with ε being arbitrarily small. This limit formally prevents the time integration from ending at the peak of a delta function. Here n_i is the outward pointing surface normal and $a_j(\mathbf{x}_r, t)$ is the particle acceleration. The subscript r in $\mathbf{x}_r$ and the superscript r in ∂_i^r indicates the receiver (recording surface) coordinates. Assuming zero initial conditions for the field and its time derivative, the last integral in equation (8) vanishes.

The retropropagated stress component $\sigma_{mn}(\mathbf{x}, t)$, with final conditions at time t^+ equal to zero, is

$$\sigma_{mn}(\mathbf{x}, t) = \int d^3x' G_{mnij}(\mathbf{x}, 0|\mathbf{x}', t) * M_{ij}(\mathbf{x}', t) + \oint_S dS(\mathbf{x}_r)\left\{ G_{mnij}(\mathbf{x}, 0|\mathbf{x}_r, t) * n_i a_j(\mathbf{x}_r, t) - [\partial_i^r G_{mnij}(\mathbf{x}, 0|\mathbf{x}_r, t)] * \frac{n_p \sigma_{jp}(\mathbf{x}_r, t)}{\rho(\mathbf{x}_r)} \right\}, \quad (9)$$

where the time integral is written as a temporal convolution (denoted $*$) for simplicity. The acoustic version of this expression, without the term proportional to $M_{ij}(\mathbf{x}, t)$, is known as the Kirchhoff integral. That is, equation (9) can be reduced to

$$P(\mathbf{x}, t) = \oint_S dS(\mathbf{x}_r)\frac{n_i}{\rho(\mathbf{x}_r)} \{G(\mathbf{x}, 0|\mathbf{x}_r, t) * [\partial_i^r P(\mathbf{x}_r, t)] - [\partial_i^r G(\mathbf{x}, 0|\mathbf{x}_r, t)] * P(\mathbf{x}_r, t)\}, \quad (10)$$

in the acoustic case if there are no internal forces in the volume V enclosed by the surface S. Here $P(\mathbf{x}, t)$ denotes pressure and $G(\mathbf{x}, t|\mathbf{x}', t')$ is the Green's function for the pressure.

To obtain an expression better suited for numerical implementation of the spatial boundary conditions, the surface integral in equation (9) can be transformed to a volume integral by application of the Dirac delta function such that

$$\sigma_{mn}(\mathbf{x}, t) = \int d^3x' G_{mnij}(\mathbf{x}, 0|\mathbf{x}', t) * M_{ij}(\mathbf{x}', t) + \int d^3x' G_{mnij}(\mathbf{x}, 0|\mathbf{x}', t) * \oint_S dS(\mathbf{x}_r) \times [\delta(\mathbf{x}' - \mathbf{x}_r) n_i a_j(\mathbf{x}_r, t) + \partial_i' \delta(\mathbf{x}' - \mathbf{x}_r) t_j(\mathbf{x}_r, t)]. \quad (11)$$

Here $t_j(\mathbf{x}_r, t)$ is the traction divided by density at receiver location $\mathbf{x}_r$,

$$t_j(\mathbf{x}_r, t) = \frac{\sigma_{ij}(\mathbf{x}_r, t) n_i}{\rho(\mathbf{x}_r)}.$$

From equation (3) and equation (11), it can be seen that $M_{ij}(\mathbf{x}, t)$ can be redefined to mean either

$$M_{ij}(\mathbf{x}, t) = \tfrac{1}{2}[\partial_i[\rho^{-1}(\mathbf{x}) f_j(\mathbf{x}, t)] + \partial_j[\rho^{-1}(\mathbf{x}) f_i(\mathbf{x}, t)]], \quad (12)$$

for representation of the internal force density, or

$$M_{ij}(\mathbf{x}, t) = \oint_S dS(\mathbf{x}_r)[\delta(\mathbf{x} - \mathbf{x}_r) n_i a_j(\mathbf{x}_r, t) + \partial_i \delta(\mathbf{x} - \mathbf{x}_r) t_j(\mathbf{x}_r, t)], \quad (13)$$

for representation of the boundary condition. This allows a unified implementation of both types of excitation functions in a finite-difference scheme through the same representation theorem

$$\sigma_{mn}(\mathbf{x}, t) = \int d^3x' G_{mnij}(\mathbf{x}, t|\mathbf{x}', 0) * M_{ij}(\mathbf{x}', t), \quad (14)$$

where $M_{ij}(\mathbf{x}, t)$ is given by equation (12) or by equation (13). The Green's tensor G_{mnij} in equation (14) must formally be replaced by the adjoint Green's tensor $\bar{G}_{mnij}$ where

$$\bar{G}_{mnij}(\mathbf{x}, t|\mathbf{x}', t') = G_{mnij}(\mathbf{x}, t'|\mathbf{x}', t), \quad (15)$$

if the field is retropropagated. Numerically this is achieved by running the modeling algorithm backward in time. The spatial form of the boundary condition is unaltered by the direction of time.

For marine surface seismic data, equation (13) in combination with equation (14) reduces to equation (10). The term proportional to $\partial_z^r P(\mathbf{x}_r, t)$ may, in principle, be obtained from a receiver deghosting, since separation in upgoing and downgoing waves is equivalent to determining the wavenumber in the z-direction, k_z^r (Cumha, 1993). The particle acceleration in equation (13) can be obtained directly in a VSP experiment by temporal differentiation of the measured particle velocity. However, the stress tensor (traction vector) is not measured for VSP data. To reconstruct the field properly for VSP data, the stress (traction) data are needed. Lacking these data is a fundamental problem that must be solved by performing the proper measurements. Measuring the full boundary condition makes it possible to determine from which side of the well a wave origites. Energy that originally came from one side of the well will be retropropagated to both sides of the well if only the particle acceleration is measured. If the formation on the far side of the well (seen from the source location) does not scatter energy back toward the well, then we know that energy is propagated in one direction through the recording surface, and from this assumption it is possible to neglect the stress part of the boundary condition. A useful solution can then be obtained in the area between the well and the source.

IMPLEMENTATION OF BOUNDARY CONDITIONS

Using high order finite difference operators (Holberg, 1987), a staggered grid approximation to the 2-D isotropic elastic wave equation at time $t = n\Delta t$ can be expressed as

$$\partial_t^2\sigma_{xx}^n(\mathbf{x}) = \lambda(\mathbf{x})[\partial_x^- A_x(\mathbf{x}) + \partial_z^- A_z(\mathbf{x}) + M_{xx}(\mathbf{x}) + M_{zz}(\mathbf{x})],$$
$$+ 2\mu(\mathbf{x})[\partial_x^- A_x(\mathbf{x}) + M_{xx}(\mathbf{x})]$$
$$\partial_t^2\sigma_{zz}^n(\mathbf{x}) = \lambda(\mathbf{x})[\partial_x^- A_x(\mathbf{x}) + \partial_z^- A_z(\mathbf{x}) + M_{xx}(\mathbf{x}) + M_{zz}(\mathbf{x})],$$
$$+ 2\mu(\mathbf{x})[\partial_z^- A_z(\mathbf{x}) + M_{zz}(\mathbf{x})]$$
$$\partial_t^2\sigma_{xz}^n(\mathbf{x}) = \mu(\mathbf{x})[\partial_x^+ A_z(\mathbf{x}) + \partial_z^+ A_x(\mathbf{x}) + M_{xz}(\mathbf{x}) + M_{zx}(\mathbf{x})], \tag{16}$$

with $\lambda(\mathbf{x})$ and $\mu(\mathbf{x})$ as the Lamé parameters. The auxiliary quantities $A_i(\mathbf{x})$ are

$$A_x(\mathbf{x}) = \rho^{-1}(\mathbf{x})[\partial_x^+\sigma_{xx}^n(\mathbf{x}) + \partial_z^-\sigma_{xz}^n(\mathbf{x})],$$
$$A_z(\mathbf{x}) = \rho^{-1}(\mathbf{x})[\partial_z^+\sigma_{zz}^n(\mathbf{x}) + \partial_x^-\sigma_{xz}^n(\mathbf{x})]. \tag{17}$$

The forward and backward derivative operators in the i-direction, ∂_i^+ and ∂_i^-, (Holberg, 1987) with operator half-length L, are given as

$$\partial_i^+\phi(x_i) = \frac{1}{\Delta x_i}\sum_{\ell=1}^{L}\alpha_\ell[\phi(x_i + \ell\Delta x_i)$$
$$- \phi(x_i - (\ell-1)\Delta x_i)] \approx \partial_i\phi(x_i + \tfrac{1}{2}\Delta x_i), \tag{18}$$

$$\partial_i^-\phi(x_i) = \frac{1}{\Delta x_i}\sum_{\ell=1}^{L}\alpha_\ell[\phi(x_i + (\ell-1)\Delta x_i)$$
$$- \phi(x_i - \ell\Delta x_i)] \approx \partial_i\phi(x_i - \tfrac{1}{2}\Delta x_i),$$

where the α_ℓ are differentiator coefficients and Δx_i is the grid step in the i-direction. Assuming that σ_{xx} and σ_{zz} are located on a reference grid, then the other field quantities are positioned as in Figure 2. The grid where σ_{xz} is located is called the shifted grid. The physical parameters are precalculated and given at the nodes where they are needed. This implies, as an example, that two representations of the same inverse density model must be given, one shifted half a grid step in the x-direction relative to the reference grid, and one shifted half a grid step in the z-direction relative to the reference grid. The time integration can be performed to a given order as described by Dablain (1986).

Two additional numerical operators are needed to proceed. The centered derivative operator ∂_i^c is given by

$$\partial_i^c\phi(x_i) = \frac{1}{\Delta x_i}\sum_{\ell=1}^{L'}\gamma_\ell[\phi(x_i + \ell\Delta x_i)$$
$$- \phi(x_i - \ell\Delta x_i)] \approx \partial_i\phi(x_i), \tag{19}$$

and the forward shift operator, ζ_i^+, is given by

$$\zeta_i^+\phi(x_i) = \sum_{\ell=1}^{L''}\beta_\ell[\phi(x_i + \ell\Delta x_i) + \phi(x_i - (\ell-1)\Delta x_i)]$$
$$\approx \phi(x_i + \tfrac{1}{2}\Delta x_i). \tag{20}$$

The latter operator calculates the field value shifted half a grid step forward in the i-direction.

In the following the 2-D discrete representation of coordinate $\mathbf{x} = (x, z)$ is given as (i, j). When discretizing the elastic wave equation with boundary conditions given by equation (13), spatially band-limited delta-functions must be introduced. The band-limited delta-function $\bar{\delta}(i - i_r, j - j_r)$ is centered on the node (i_r, j_r) on the reference grid. This delta-function can be any band-limited approximation to the Dirac delta function; the only restriction is that no wavenumber is higher than the spatial Nyquist frequency. In this calculation, it is assumed that $\bar{\delta}(i - i_r, j - j_r)$ is a 2-D sinc function such that

$$\bar{\delta}(i - i_r, j - j_r) = \begin{cases} \dfrac{1}{\Delta x}\dfrac{1}{\Delta z} & \text{if } i = i_r \text{ and } j = j_r \\ 0 & \text{otherwise} \end{cases}, \tag{21}$$

on the reference grid.

From equation (13) in combination with equation (16), it can be seen that discrete approximations to the delta-function and its first order partial derivatives on the reference grid and on the shifted grid are needed. The functions $\mathcal{D}^R(i - i_r, j - j_r)$, $\mathcal{D}_x^R(i - i_r, j - j_r)$, and $\mathcal{D}_z^R(i - i_r, j - j_r)$ are the representations of this band-limited delta function and its first-order derivatives on the reference grid. These discretized functions have an odd number of elements $(2K + 1)$ in both i- and j-directions since they are centered on the node (i_r, j_r) on the reference grid. The functions $\mathcal{D}^S(i - i_r, j - j_r)$, $\mathcal{D}_x^S(i - i_r, j - j_r)$, and $\mathcal{D}_z^S(i - i_r, j - j_r)$ are the representations of $\bar{\delta}(i - i_r, j - j_r)$ and its first-order derivatives on the shifted grid. These discretized functions have an even number of elements $(2M)$ in both i- and

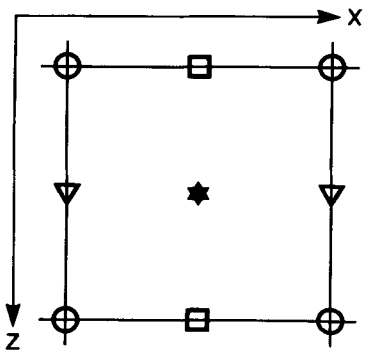

○ :	σ_{xx}, σ_{zz}	λ_0, μ_0	$\mathcal{D}^R, \mathcal{D}_x^R\mathcal{D}_z^R$
✸ :	σ_{xz}	μ_3	$\mathcal{D}^S, \mathcal{D}_x^S\mathcal{D}_z^S$
□ :	A_x	ρ_1^{-1}	
▽ :	A_z	ρ_2^{-1}	

FIG. 2. σ_{xx} and σ_{zz} are located on a reference grid. A_x is shifted systematically half a grid step in the x-direction relative to the reference grid. A_z is shifted systematically half a grid step in the z-direction relative to the reference grid, and σ_{xz} is shifted half a grid step in both the x- and z-directions relative to the reference grid.

j-directions since they are also centered on the node (i_r, j_r) on the reference grid.

Hence, I propose to use the following band-limited spatial distribution functions when implementing the boundary conditions,

$$\begin{aligned}
\mathcal{D}^R(i-i_r, j-j_r) &= \bar{\delta}(i-i_r, j-j_r),\\
\mathcal{D}^R_x(i-i_r, j-j_r) &= \partial_x^c\bar{\delta}(i-i_r, j-j_r),\\
\mathcal{D}^R_z(i-i_r, j-j_r) &= \partial_z^c\bar{\delta}(i-i_r, j-j_r),\\
\mathcal{D}^S(i-i_r, j-j_r) &= \zeta_x^+\zeta_z^+\bar{\delta}(i-i_r, j-j_r),\\
\mathcal{D}^S_x(i-i_r, j-j_r) &= \partial_x^+\zeta_z^+\bar{\delta}(i-i_r, j-j_r),\\
\mathcal{D}^S_z(i-i_r, j-j_r) &= \zeta_x^+\partial_z^+\bar{\delta}(i-i_r, j-j_r).
\end{aligned} \tag{22}$$

In the numerical implementation the size of the band-limited functions given in equation (22) are such that K and M may vary from 1 to 8.

For the examples given in this paper, a scheme that is second order in time is used. The elastic wave equation may then be solved by first calculating $A_i(i, j)$, that is

$$\begin{aligned}
A_x(i, j) &= \rho_1^{-1}(i, j)[\partial_x^+\sigma^n_{xx}(i, j) + \partial_z^-\sigma^n_{xz}(i, j)],\\
A_z(i, j) &= \rho_2^{-1}(i, j)[\partial_z^+\sigma^n_{zz}(i, j) + \partial_x^-\sigma^n_{xz}(i, j)],
\end{aligned} \tag{23}$$

where $\rho_1^{-1}(i, j)$ is the inverse density model shifted half a grid step in the x-direction relative to the reference density model and $\rho_2^{-1}(i, j)$ is the inverse density model shifted half a grid step in the z-direction relative to the reference density model.

The following expressions are obtained when $M_{pq}(\mathbf{x}, t)$ (let $M_{pq}(\mathbf{x}, t) \to M^n_{pq}(i, j)$) is assumed to be of the form given in equation (13),

$$\begin{aligned}
\partial_t^2\sigma^n_{xx}(i, j) &= \lambda_0(i, j)[\partial_x^-A_x(i, j) + \partial_z^-A_z(i, j) + M^n_{xx}(i, j)\\
&\quad + M^n_{zz}(i, j)] + 2\mu_0(i, j)[\partial_x^-A_x(i, j) + M^n_{xx}(i, j)],\\
\partial_t^2\sigma^n_{zz}(i, j) &= \lambda_0(i, j)[\partial_x^-A_x(i, j) + \partial_z^-A_z(i, j) + M^n_{xx}(i, j)\\
&\quad + M^n_{zz}(i, j)] + 2\mu_0(i, j)[\partial_z^-A_z(i, j) + M^n_{zz}(i, j)],
\end{aligned} \tag{24}$$

with

$$\begin{aligned}
M^n_{xx}(i, j) &= \sum_{i_r, j_r}\{\mathcal{D}^R(i-i_r, j-j_r)n_x(i_r, j_r)a^n_x(i_r, j_r)\\
&\quad + \mathcal{D}^R_x(i-i_r, j-j_r)t^n_x(i_r, j_r)\}\,\Delta S(i_r, j_r),\\
M^n_{zz}(i, j) &= \sum_{i_r, j_r}[\mathcal{D}^R(i-i_r, j-j_r)n_z(i_r, j_r)a^n_z(i_r, j_r)\\
&\quad + \mathcal{D}^R_z(i-i_r, j-j_r)t^n_z(i_r, j_r)]\,\Delta S(i_r, j_r).
\end{aligned} \tag{25}$$

The off-diagonal stress component can be expressed

$$\begin{aligned}
\partial_t^2\sigma^n_{xz}(i, j) &= \mu_3(i, j)[\partial_x^+A_z(i, j) + \partial_z^+A_x(i, j)\\
&\quad + M^n_{xz}(i, j) + M^n_{zx}(i, j)],
\end{aligned} \tag{26}$$

with

$$\begin{aligned}
M^n_{xz}(i, j) &= \sum_{i_r, j_r}[\mathcal{D}^S(i-i_r, j-j_r)n_x(i_r, j_r)a^n_z(i_r, j_r)\\
&\quad + \mathcal{D}^S_x(i-i_r, j-j_r)t^n_z(i_r, j_r)]\,\Delta S(i_r, j_r),\\
M^n_{zx}(i, j) &= \sum_{i_r, j_r}[\mathcal{D}^S(i-i_r, j-j_r)n_z(i_r, j_r)a^n_x(i_r, j_r)\\
&\quad + \mathcal{D}^S_z(i-i_r, j-j_r)t^n_x(i_r, j_r)]\,\Delta S(i_r, j_r).
\end{aligned} \tag{27}$$

Here $\lambda_0(i, j)$ and $\mu_0(i, j)$ are located on the reference grid and $\mu_3(i, j)$ is located on the shifted grid. The surface element is given by $\Delta S(i_r, j_r)$.

NUMERICAL EXAMPLE

To test the implementation of the boundary conditions, a 2-D numerical experiment was performed. The model is shown in Figure 1. The medium is homogeneous with P-wave velocity equal to 2000 m/s, S-wave velocity equal to 1200 m/s, and density equal to 2.0 g/cm^3. The source position is marked with a star in Figure 1. The source generates both a P-wave and an S-wave with a maximum frequency of 40 Hz. The spatial steplengths are 10 m in both x- and z-directions. The half-length L of the spatial derivative operators in equation (19) is equal to 6. The top edge of the computational grid is an elastic-free surface and there are absorbing boundaries around the other three edges of the grid.

First a forward modeling was performed. The components of the forward modeled field required to reconstruct the field in a reverse time modeling were shifted to the reference grid and recorded along the surface S. These components, $a^n_x(i_r, j_r)$, $a^n_z(i_r, j_r)$, $t^n_x(i_r, j_r)$, and $t^n_z(i_r, j_r)$, are used as boundary conditions, in accordance with equation (11), when performing a reverse-time modeling of the wavefield. The size of the spatial delta functions and their first-order derivatives are such that both $K = 6$ and $M = 6$. This is the length used for the derivative operators, so both approximations have the same spatial bandwidth.

The interface S in Figure 1 has both plane and curved parts. It is important to test both types of boundaries. Even for a planar interface, the staggering of the grid may cause problems. The implementation of the boundary condition must obey the rules given by the staggering of the grid or else the boundary will have a sawtooth appearance. The representation theorem has a fine balance of constructive and destructive interference such that the field is reconstructed on one side of the boundary (inside S in the example given here), whereas it is zero on the other side of the boundary. A sawtooth implementation of the boundary condition will

FIG. 3. Snapshots of the a_z-component of the forward-modeled field. The source generates both a P-wave and an S-wave. The first snapshot is for time equal to 0.3 s and the last snapshot is for time equal to 3.1 s. The wave marked "p" is the direct P-wave; the wave marked "s" is the direct S-wave. The wave marked "pp" is the P-wave reflection of the direct P-wave. The wave marked "ps" is the S-wave reflection of the direct P-wave. The wave marked "sp" is the P-wave reflection of the direct S-wave. The wave marked "ss" is the S-wave reflection of the direct S-wave.

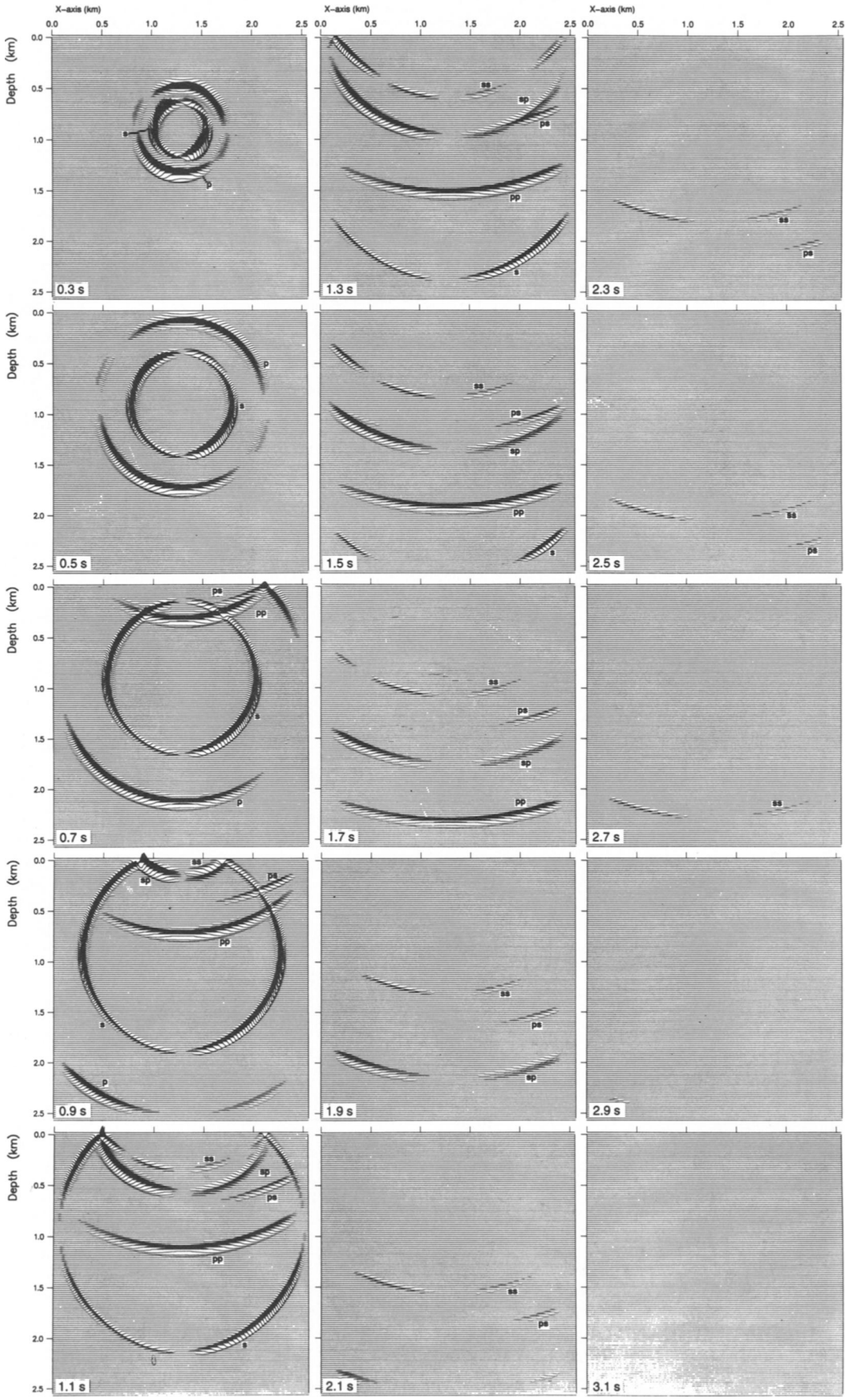

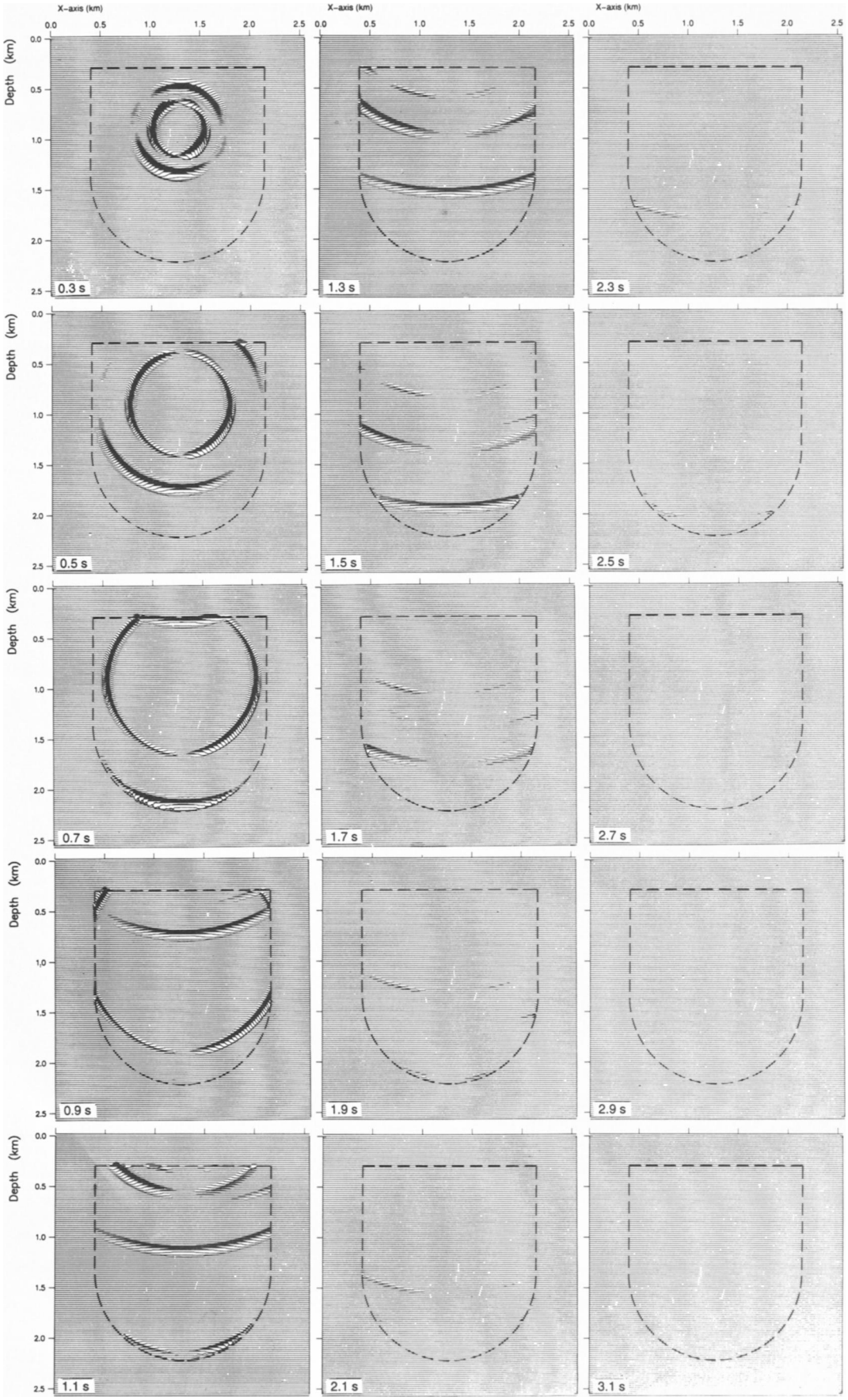

FIG. 4. Snapshots of the a_z-component of the retropropagated field. The field is reconstructed inside the surface S only, which is in agreement with theory.

destroy this fine balance and false P- and S-waves will be generated on both sides of the boundary.

Snapshots of the a_z-component are shown in Figure 3 with the direct and reflected events marked. The snapshots of the a_z-component for the reverse-time modeling are shown in Figure 4. The scaling is the same for Figure 3 and Figure 4. It can be observed from Figure 4 that inside the closed surface S, all events are recovered for the reconstructed field, whereas the field is zero outside this surface. The numerical artifacts from the spatial implementation of the boundary conditions are negligible. This is further confirmed in Figure 5, which shows the difference of the forward modeled a_z-component and the retropropagated a_z-component at time 1.3 s. The difference between the two data sets is nonzero outside the surface S only. This implies that the field is satisfactorily reconstructed with the spatial boundary conditions given by equation (22) when performing reverse-time modeling. It is also clear that both correct amplitude and phase of the field are recovered inside S.

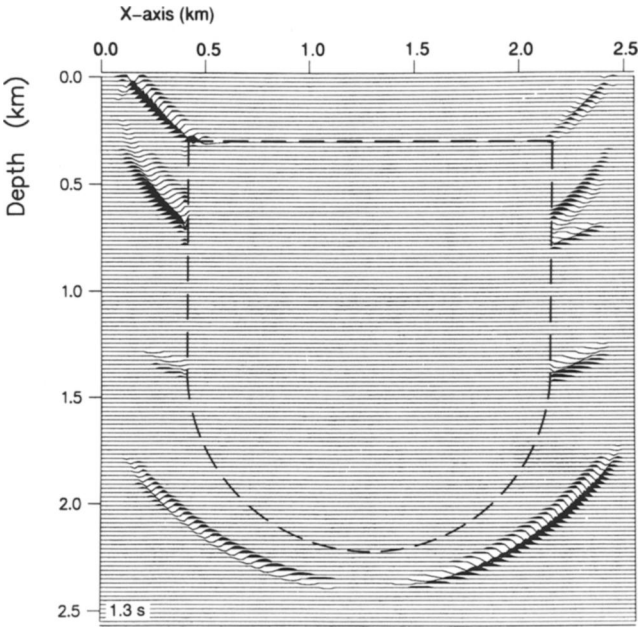

FIG. 5. The difference of the forward-modeled a_z-component and the retropropagated a_z-component. The difference between the two data sets is nonzero outside the surface S only. This implies that the field is satisfactorily reconstructed by reverse-time modeling with correct amplitude and phase inside S.

CONCLUSION

It has been demonstrated how the spatial part of the boundary condition for an elastic field can be implemented numerically in a staggered coarse grid modeling scheme with good accuracy by using band-limited spatial delta functions and band-limited, first-order derivatives of these spatial delta functions. The numerical implementation of the boundary condition was tested in a numerical experiment for a closed but curved boundary. Both P- and S-waves were properly recovered in the reverse-time modeling operation. The numerical artifacts related to the spatial approximation of the boundary condition were negligible.

ACKNOWLEDGMENTS

Thanks to Olav Holberg who has designed the coefficients of the numerical derivative and shift operators. I also thank Lasse Amundsen and Børge Arntsen for stimulating discussions on implementation of the representation theorem for coarse grid numerical schemes.

REFERENCES

Aki, K., and Richards, P. G., 1980, Quantitative seismology: W. H. Freeman and Co.

Chang, W. F., and McMechan, G. A., 1986, Reverse-time migration of offset vertical seismic profiling data using the excitation-time imaging condition: Geophysics, **51**, 67–84.

Cumha, C. A., 1993, Transforming marine pressure data into a vector wavefield: 63rd Ann. Internat. Mtg., Soc. Expl. Geophys., Expanded Abstracts, 1060–1064.

Dablain, M. A., 1986, The application of higher-order differencing to the scalar wave equation: Geophysics, **51**, 54–66.

Fornberg, B., 1990, High-order finite differences and the pseudospectral method on staggered grids: SIAM J. Num. Anal., **27**, 904–918.

Gazdag, J., 1981, Modeling of the acoustic wave equation with transform methods: Geophysics, **46**, 854–859.

Holberg, O., 1987, Computational aspects of the choice of operator and sampling interval for numerical differentiation in large-scale simulation of wave phenomena: Geophys. Prosp., **35**, 629–655.

Kosloff, D. D., and Baysal, E., 1982, Forward modeling by a Fourier method: Geophysics, **47**, 1402–1412.

Levander, A. R., 1988, Fourth-order finite-difference P-SV seismograms: Geophysics, **53**, 1425–1436.

Madariaga, R., 1976, Dynamics of an expanding circular fault: Bull. Seis. Soc. Am., **66**, 163–182.

Mittet, R., and Helgesen, J., 1992, Elastic iterative migration of offset VSP data: 62nd Ann. Internat. Mtg., Soc. Expl. Geophys., Expanded Abstracts, 984–987.

Morse, P. M., and Feshbach, H., 1953, Methods of theoretical physics: McGraw-Hill Book Co.

Virieux, J., 1984, SH-wave propagation in heterogeneous media: Velocity-stress finite-difference method: Geophysics, **49**, 1933–1957.

——— 1986, P-SV-wave propagation in heterogeneous media: Velocity-stress finite-difference method: Geophysics, **51**, 889–901.